JOURNAL OF SPACECRAFT AND ROCKETS
Vol. 46, No. 4, July–August 2009

Dynamic Simulations of Atmospheric-Entry Capsules

Scott M. Murman*
NASA Ames Research Center, Moffett Field, California 94035

DOI: 10.2514/1.41078

Viscous free-oscillation simulations with the OVERFLOW solver are used to predict the aerodynamic behavior of nonlifting capsule shapes in the supersonic-speed regime. Computations using hybrid Reynolds-averaged Navier–Stokes turbulence models are examined for two novel atmospheric-entry capsule configurations: an idealized inflatable decelerator concept and the Orion crew module. The simulation results are validated against nonlinear aerodynamic models determined from free-flight ballistic-range data analysis. For the Orion crew module, two separate methods of reducing identical range data, along with common models tested in separate range facilities, are included. The computations demonstrate the efficiency and accuracy of dynamic simulations for developing a nonlinear aerodynamic performance database. Analysis indicates that the typical nonlinear bluff-body behavior is characterized by a rate-dependent dynamic response, which is not currently accounted for in common aerodynamic models.

Nomenclature

a	=	sonic speed
C_A, C_N, C_Y	=	axial, normal, and lateral force coefficients
$\boldsymbol{C}_F$	=	aerodynamic loads
C_l, C_m, C_n	=	roll, pitch, and yaw moment coefficients
$\boldsymbol{e}$	=	error
M	=	Mach number
p, q, r	=	roll, pitch, and yaw rates
Re	=	Reynolds number
t	=	time
$\boldsymbol{u}$	=	velocity
α	=	angle of attack, deg
$\dot{\alpha}$, $\dot{\beta}$	=	rate of change of α and β
β	=	angle of sideslip, deg
δ_i	=	control-surface settings
$\boldsymbol{\eta}$	=	dynamic aerodynamic parameters
$\boldsymbol{\xi}$	=	static aerodynamic parameters
σ	=	standard deviation

Subscripts

d	=	dynamic derivative
o	=	base state
s	=	static derivative
tot	=	total (axisymmetric) angle
∞	=	freestream

I. Introduction

COMPUTATIONAL fluid dynamics (CFD) is a key technology in the design of NASA's Orion crew module (CM) entry capsule and in the development of novel high-mass decelerator concepts for future Mars missions. Atmospheric-entry capsule and probe shapes provide a challenge for numerical analysis due to the inevitable separation and bluff-body shedding over the aft end of the vehicle. This same unsteady physics creates difficulties for stability and control, as the pitch damping is adversely effected when it is most needed to damp the oscillations, due to the unsteady wake. Further, accurately determining the pitch damping from experimental measurements for capsule and probe shapes has been a challenge dating back to the Apollo and Viking programs (cf. [1–7]). This paper uses viscous moving-body (free-oscillation) CFD simulations to predict the aerodynamic behavior of capsule shapes in the supersonic-speed regime. These simulations provide both the static and dynamic coefficients needed for accurate aerodynamic modeling of performance, risk assessment, targeting, etc.

Previous work used an automated Cartesian-mesh-based inviscid flow solver to perform a dynamic analysis for the Viking, Mars Exploration Rover, and Genesis sample-return capsule at supersonic flow conditions [8]. This work extends that effort to viscous Reynolds-averaged Navier–Stokes (RANS) simulations of two novel capsule shapes using the OVERFLOW solver [9–11] and validates the results against recent free-flight ballistic-range data. The configurations analyzed are an inflatable aerodynamic decelerator concept for Mars entry developed by NASA's Program to Advance Inflatable Decelerators for Atmospheric Entry (PAI-DAE) [12] and the Orion CM [13–15]. The former is referred to herein as simply the PAI-DAE configuration and is modeled as a rigid aeroshell to match the rigid ballistic-range test model. The outer mold line for these configurations is presented in Fig. 1. Both are analyzed at supersonic ballistic-entry (nonlifting) conditions.

To generate aerodynamic coefficient data from free-flight testing, an a priori assumption of the aerodynamic model (i.e., parameter and system identification) is necessary. This modeling effort is combined with regression methods to reduce free-flight observations (position and orientation) to aerodynamic coefficients. These modeling and regression choices are not unique, however, and the issues associated with aerodynamic modeling of ballistic-range experiments (viz, the validation of simulation results) must be considered. The paper thus begins with a review of aerodynamic modeling, focusing on the analysis of supersonic bluff-bodies and the methods used in both ballistic range and CFD data reduction.

The discussion continues with a brief overview of the numerical approach, followed by analyses of the PAI-DAE and Orion capsules using hybrid-RANS simulation methods and comparison with free-flight range data. A summary of the major points from the current work concludes the paper.

II. Aerodynamic Modeling

The aerodynamic characteristics of an aircraft are typically described by the force and moment coefficients about the body axes: the axial, normal, and lateral force coefficients (C_A, C_N, and C_Y) and the roll, pitch, and yaw moment coefficients (C_l, C_m, and C_n). Adopting a vector notation, the body force and moments are

Presented as Paper 6911 at the 26th AIAA Applied Aerodynamics Conference, Honolulu, HI, 18–21 August 2008; received 17 September 2008; revision received 15 January 2009; accepted for publication 26 January 2009.

*Aerospace Engineer; Scott.M.Murman@nasa.gov. Member AIAA.

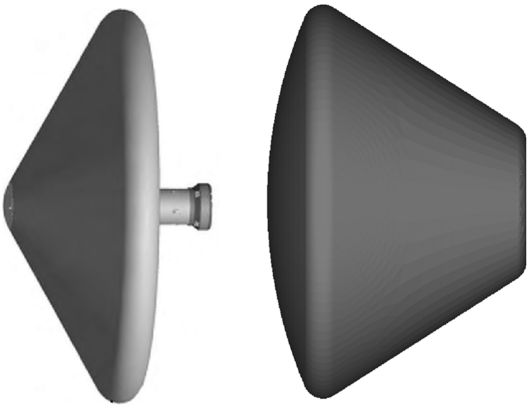

a) PAI-DAE b) Orion CM

Fig. 1 Outer mold lines for the atmospheric-entry capsule shapes analyzed in this work. These shapes correspond to idealized subscale ballistic-range models [12,13].

$$\hat{\boldsymbol{C}}_F = [C_A, C_N, C_Y, C_l, C_m, C_n]^T \tag{1}$$

In this work, the aerodynamic coefficients are considered as functions of solely the flight conditions and aircraft configuration:

$$\hat{\boldsymbol{C}}_F = \hat{\boldsymbol{C}}_F(\alpha, \beta, M_\infty, \delta_i, p, q, r, \dot{\alpha}, \dot{\beta}) \tag{2}$$

where δ_i represents any configuration-dependent information such as control-surface settings, and p, q, and r are the roll, pitch, and yaw rotation rates, respectively.[†] A more detailed representation would potentially include dependencies on altitude, propulsion, etc., which can be treated in a similar manner, but are not necessary for the current discussion. It is assumed here that for any numerical simulation, each independent variable is specified exactly, and the resulting computed aerodynamic forces and moments will have associated errors and uncertainties. We thus distinguish the computed forces and moments as $\boldsymbol{C}_F$, which differ from the exact values by an error distribution $\hat{\boldsymbol{C}}_F = \boldsymbol{C}_F + \boldsymbol{e}$.

Theoretically, the aerodynamic loads can be tabulated as functions of all the independent parameters, with suitable resolution in regions of rapid variation. In practice, the effects of the dynamic parameters p, q, r, $\dot{\alpha}$, and $\dot{\beta}$ are usually isolated using a linear expansion. Adopting $\boldsymbol{\xi}$ and $\boldsymbol{\eta}$ to represent the vectors of static and dynamic parameters, respectively, we then have

$$\begin{aligned}\hat{\boldsymbol{C}}_F(\boldsymbol{\xi}, \boldsymbol{\eta}) &= \boldsymbol{C}_F(\boldsymbol{\xi}, \boldsymbol{\eta}) + \boldsymbol{e} = \boldsymbol{C}_F(\boldsymbol{\xi})|_{\boldsymbol{\eta}=0} + \frac{\partial \boldsymbol{C}_F}{\partial \boldsymbol{\eta}}(\boldsymbol{\xi})\Delta\boldsymbol{\eta} + \boldsymbol{e} \\ &= \boldsymbol{C}_{F_s}(\boldsymbol{\xi}) + \boldsymbol{C}_{F_d}(\boldsymbol{\xi})\Delta\boldsymbol{\eta} + \boldsymbol{e}\end{aligned} \tag{3}$$

In Eq. (3) we now also have a *fit error* included in $\boldsymbol{e}$, which measures how well the linear expansion fits the data. Here, we refer to $\boldsymbol{C}_{F_d}$ as the dynamic coefficients and to $\boldsymbol{C}_{F_s}$ as the static coefficients. Note that these static coefficients are not, in general, identical to the results of static simulations. The motivation for Eq. (3) is that both the static and dynamic coefficients are now only functions of the static parameters, $\boldsymbol{\xi}$ and are hence easier to either tabulate or model.

As a more concrete example, we examine the pitching moment obtained from a free-oscillation simulation. For this 1-DOF simulation, the two independent parameter vectors reduce to $\boldsymbol{\xi} = \alpha$ and $\boldsymbol{\eta} = q$.[‡] Simplifying Eq. (3), and only considering pitching moment, we thus have

$$\hat{C}_m(\alpha, q) = C_{m_s}(\alpha) + C_{m_d}(\alpha)\Delta q + e \tag{4}$$

[†]It is assumed that the rotation rates are suitably nondimensionalized. The set of rotational parameters is often reduced using linear combinations: for example, combining the effects of pitching and plunging as $\frac{1}{2}(q + \dot{\alpha})$ (cf. Kalviste [16]).

[‡]The values of $\dot{\alpha}$ and q are equivalent for a free-oscillation motion.

Figure 2 presents the variation of pitching moment with time and pitch rate for a representative free-oscillation simulation. The coefficients from Eq. (4) are labeled in Fig. 2 for clarity. Both C_{m_s} and C_{m_d} are calculated directly by a linear regression against the computed data.[§] Further, modeling of the coefficients to facilitate analysis and the development of guidance and control systems is possible. For example, a linear aerodynamic model is constructed using

$$C_{m_s}(\alpha) = C_{m_\circ} + \frac{\partial C_m}{\partial \alpha}\Delta\alpha = C_{m_\circ} + C_{m_\alpha}\Delta\alpha \tag{5}$$

$$C_{m_d}(\alpha) = \frac{\partial C_m}{\partial q} = C_{m_q} \tag{6}$$

where C_{m_α} is the pitch stiffness, and C_{m_q} is the pitch damping. Combining Eqs. (5) and (6) with Eq. (4) gives

$$\hat{C}_m(\alpha, q) = C_{m_\circ} + C_{m_\alpha}\Delta\alpha + C_{m_q}\Delta q + e \tag{7}$$

where the aerodynamic coefficients are commonly determined from a multiple linear regression.

In ballistic-range testing, the aerodynamic coefficients are not typically measured directly, but rather inferred from an assumed aerodynamic model that is fit against the measured trajectory of the test article. For example, in reducing atmospheric-entry capsule configurations, Chapman and Yates [5] assume the following forms[¶] for the static and dynamic coefficients in Eq. (4),

$$C_{m_s}(\alpha) = C_{m_\circ} + C_{m_\alpha}\sin\alpha + C_{m_{\alpha^3}}\sin^3\alpha \tag{8}$$

$$C_{m_d}(\alpha) = C_{m_q} + (C_{m_q})_{\alpha^2}\sin^2\alpha \tag{9}$$

along with a data-partitioning process. This data-reduction process creates a difficulty for the validation of CFD results against free-flight data. As the free-flight data-reduction methods increase in complexity, replicating them becomes impractical, and so comparisons of computed and test results necessarily contain ambiguity in the reported quantities. The modeling forms are also not unique, with several plausible choices replicating the limited number [$\mathcal{O}(10)$] of experimental runs, and engineering judgment of the ballistic-range data analyst is currently the deciding factor. The CFD simulations of the Orion CM in Sec. V are compared against two separate experimental data-reduction methods of a single ballistic-range data set, as well as data from two distinct range facilities using the same data-reduction process.

An a priori aerodynamic modeling assumption is similarly necessary to reduce CFD free-flight simulation results to aerodynamic coefficients. The current work avoids this issue by focusing solely on free-oscillation simulations in which the vehicle is pinned through the center of mass and only allowed to rotate in the pitch plane. The data-reduction process then simplifies to a linear (dynamic) expansion in the pitch plane [e.g., Eq. (4)], in which the nonlinear static and dynamic coefficients are tabulated for comparison against the nonlinear ballistic-range models.

III. Numerical Method

OVERFLOW provides an attractive testbed for the current study, due to the large number of turbulence models included in the standard distribution and the ease with which new models can be added. One of the goals of this work is to evaluate the predictive capability of current engineering CFD tools for dynamic analysis. As such, the same procedure is used for each configuration analyzed in this work.

[§]The uncertainty e is commonly assumed to be a normal distribution with zero mean, and so the regression analysis is equivalent to a maximum likelihood estimate.

[¶]For simplicity, this discussion neglects contributions outside the pinned 1-DOF pitching motion and focuses on ballistic configurations that trim about $\alpha = 0$ deg.

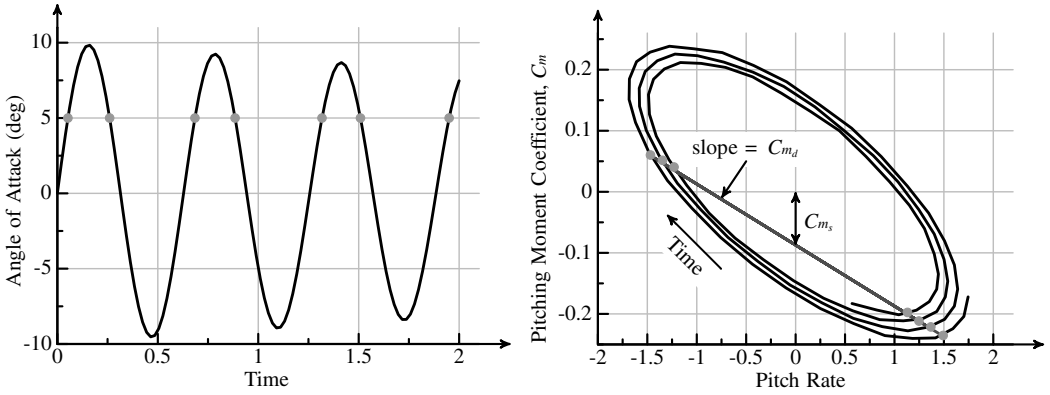

Fig. 2 Typical free-oscillation simulation data. Roughly 50 time steps resolve each period of oscillation using a second-order numerical scheme. The $\alpha = 5$ deg points are highlighted in both figures, and the static and dynamic coefficients determined from a linear regression of Eq. (4) are shown.

OVERFLOW's default central-differencing scheme with scalar artificial dissipation model is used throughout. The dynamic simulations use the Spalart–Allmaras detached-eddy simulation (DES) turbulence model [17]. Grid refinement studies using the DES model do not lead to grid convergence, as the physical model itself (filter width) changes with mesh resolution. Hence, the spatial resolution is determined from a grid sensitivity study at static conditions using Olsen and Coakley's [18] k-ω lag RANS turbulence model. This approach has been used previously for static simulations in the supersonic regime for the Apollo and Orion CM capsules [19,20]. A typical overset viscous mesh resulting from this resolution study contains between 9.5–11 million cells. A sample cutting surface through the pitch plane of the computational mesh for the Orion CM, along with computed Mach contours at Mach 1.25, is shown in Fig. 3. Body-conforming regions are used to capture the boundary layer, with automatic Cartesian meshing outside these regions. The mesh is generated automatically from the analytical outer mold-line definitions using a derivative of the Chimera Grid Tools [21] script developed by Chaderjian and Olsen [19].

The current work uses free-oscillation simulations in which the vehicle is pinned through the center of mass and only allowed to rotate in the pitch plane in response to the aerodynamic torque. This leverages the inertia of the body to filter the nonlinear response of the wake (cf. [8]) and provides an accurate model of the dynamic response. In this method, the computational mesh is fixed, and the entire domain rotates with the body. The inertia and dimensions of the configurations match the ballistic-range test articles. Above Mach 1.5, the supersonic flow damps much of the unsteady wake shedding, and a time resolution of 50 time steps per body oscillation period with the second-order backward time-integration scheme is used. Using the boundary-layer acceleration described in [22], 50–100 dual-time subiterations are required at each time step to converge the skin friction for this temporal resolution. Below Mach 1.5, the unsteady wake contains a broader range of scales, and a time-resolution study is necessary. The current approach uses static unsteady simulations with varying time resolution until the prediction of axial force converges. This procedure typically leads to 500 time steps per oscillation period at the low supersonic Mach numbers. A dynamic simulation with 10 million cells requires roughly 100 Itanium 2 CPU hours per oscillation cycle, and a minimum of three oscillation cycles is desired.

IV. PAI-DAE

NASA's PAI-DAE project researches methods to replace canopy decelerators with attached inflatable drag devices to increase the mass that can safely be landed during atmospheric entry: most notably, on Mars, for which the density of the atmosphere limits traditional decelerator technologies (cf. Hughes et al. [23]). The configuration examined here is one of a parametric series of rigid models (approximating a stacked-toroid concept) tested in the Aeroballistic Research Facility (ARF) at Eglin Air Force Base [12]. The aerodynamic coefficients are reduced from shadowgraph images using the Comprehensive Aerodynamic Data Reduction System for Aeroballistic Ranges (CADRA) software developed by Yates [24]. The pitch plane of the computational mesh for the PAI-DAE model is shown Fig. 4, along with computed Mach contours. The model is a 60 deg sphere-cone forebody with a concave aftbody and cylindrical base. This model is chosen because it contains the greatest number of experimental data points (4) of the 60 deg forebody configurations tested.

Free-oscillation simulations of the PAI-DAE configuration at supersonic conditions using the OVERFLOW RANS solver with the Spalart–Allmaras DES turbulence model [17] are presented. The DES model includes the low-Reynolds-number corrections for wake flows [25]. Figure 5 compares the computed aerodynamic

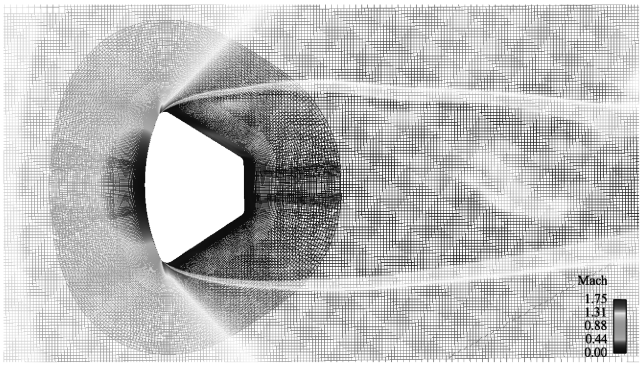

Fig. 3 Overset computational mesh and Mach contours along the lateral symmetry plane for the Orion CM configuration; volume mesh contains 11 million grid points ($M_\infty = 1.25$, $\alpha \approx 0$ deg, and $Re_D = 1.75 \times 10^6$).

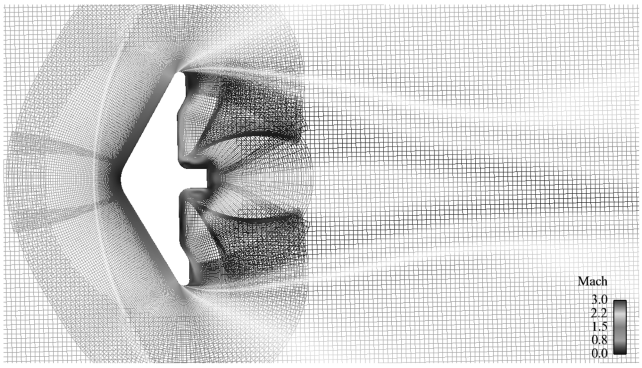

Fig. 4 Overset computational mesh and Mach contours along the lateral symmetry plane for a rigid sphere-cone PAI-DAE configuration; volume mesh contains 9.8 million grid points ($M_\infty = 2.5$, $\alpha \approx 0$ deg, and $Re_D = 4.1 \times 10^6$).

coefficients against data reductions from the ballistic-range trajectories. Uncertainties ($\pm 3\sigma$) for the experimental regression fit are included using the error estimates from the range data and assuming a uniform error distribution. Note that these do not represent cumulative experimental uncertainties. Two separate simulations are included for each Mach number, with the body released from both 15 and 5 deg from the static trim point ($\alpha = 0$ deg). The range data include two high-amplitude trajectories, with oscillations through ± 10 deg in total angle of attack, and two lower-amplitude ($\alpha_{\text{tot}} < \pm 5$ deg) trajectories. The simulation and free-flight drag coefficient are in good agreement at all Mach numbers. The range data regression does not include a dynamic component for the drag coefficient, whereas the simulations indicate a noticeable hysteresis at $M_\infty = 1.5$. The oscillation of the unsteady wake is also evident in the drag variation at $M_\infty = 1.5$, and resolving this feature is required for accurate predictions. At the lower speed, the greater load increment due to the stronger wake causes oscillations in the computed damping predictions. The static pitching-moment coefficient is in good agreement, though slightly underpredicts the slope of the range data regression at the higher speeds. The dynamic pitching-moment coefficient demonstrates two trends, differing with release angle of attack. The release 15 deg from the static trim point is in good agreement with the range predictions for the higher angles of attack, but underpredicts the dynamic instability near the static trim point. The lower-angle-of-attack release does predict a noticeably greater instability, however. Note that at the peak amplitude of the oscillation, the rotation rate is essentially zero and the dynamic coefficient is arbitrary.

For the Mach 2.5 simulations in Fig. 5, two $\alpha = 15$ deg releases are included in the dynamic coefficient, one that resolves the dynamics using roughly 50 time steps per oscillation period and one that matches the angular resolution of the lower-angle-of-attack release. There are no significant differences in the predicted pitch damping with angular resolution, indicating that the changing behavior with release angle of attack is not numerical in origin. Teramoto et al. [26] and Teramoto and Fuji [27] note similar dynamic phase delays in the pressure field about a capsule computed at transonic conditions. One of the significant differences between the low- and high-angle-of-attack releases is the rotation rate passing through the static trim point, with the higher-amplitude release resulting in roughly twice the pitch rate. The next section discusses physical mechanisms that lead to the change in aerodynamic damping with release angle of attack. The larger issue is the assumption inherent in commonly used aerodynamic models (including those of the ballistic-range data reduction) that the dynamic coefficients are independent of rotation rate [e.g., Eq. (3)]. Based on the simulation data here (and the next section), this assumption should be reconsidered, and refined models that account for a more general dynamic increment may be necessary for these nonlinear bluff-body flows.

The computed aerodynamic predictions in Fig. 5 represent a cumulative cost of roughly 2000 CPU hours on the NASA SGI Altix Columbia system (3 Mach numbers, by 2 simulations, by 300 CPU

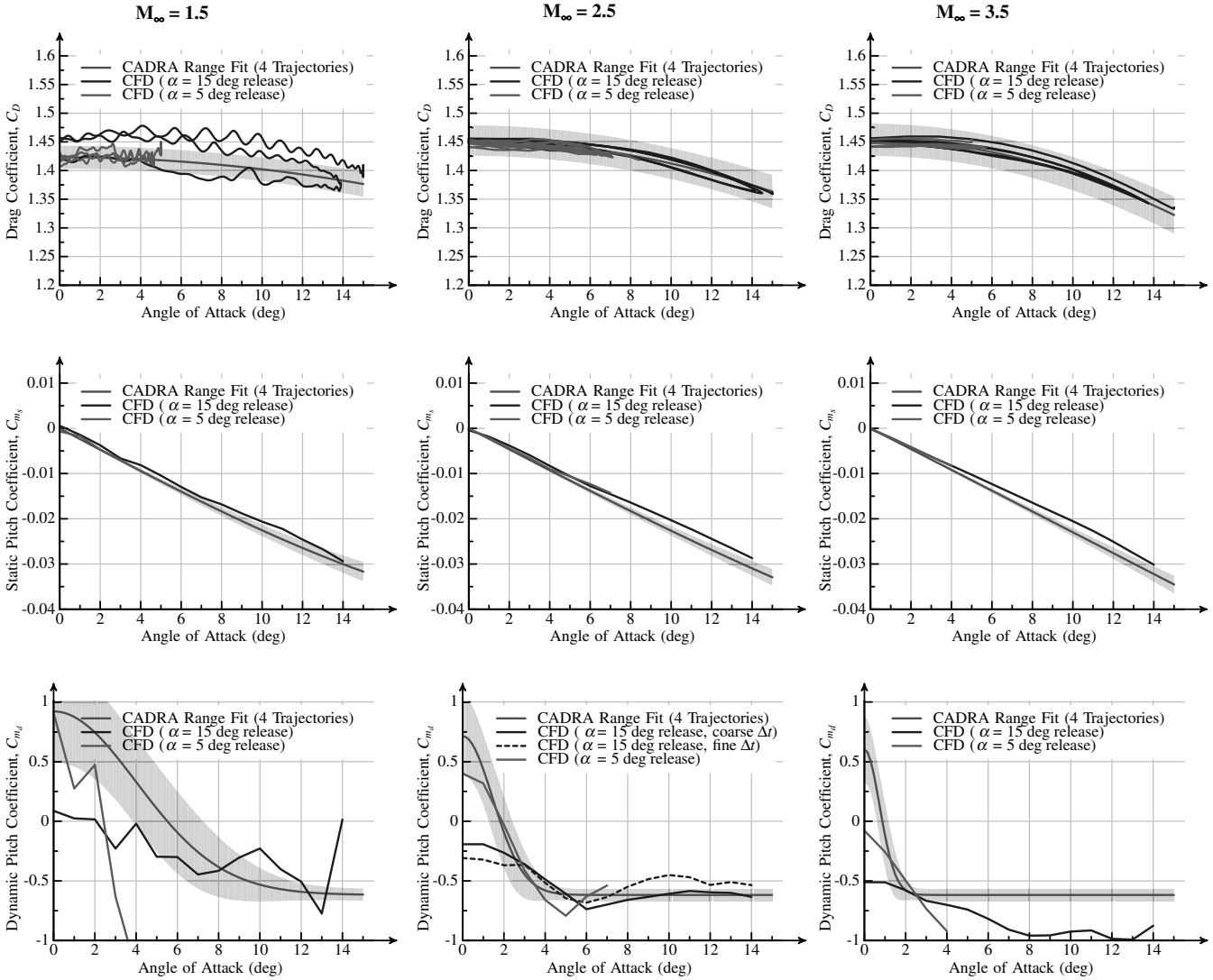

Fig. 5 Predictions of the static and dynamic (C_D, C_{m_s}, and C_{m_d}) aerodynamic coefficients for a rigid sphere-cone PAI-DAE configuration at three supersonic Mach numbers. Range data are the regression fit of an assumed aerodynamic model against the trajectory data [12], and 3σ uncertainties are included for the range data regression fit by assuming a uniform error distribution.

hours per simulation). From this investment, accurate predictions of both the static and dynamic response coefficients are obtained. The dynamic simulation approach is thus computationally efficient, requiring a fraction of the resources of a typical static database approach. For inherently unsteady flows, a static database requires time-averaged unsteady simulation results at each point in the parameter space and does not provide any dynamic response information.

V. Orion Crew Module

Extensive ballistic-range and wind-tunnel test data exist for the Orion CM, in both lifting and nonlifting configurations, from supersonic through subsonic speeds. The comparisons here are at supersonic (approximately flight Reynolds number) conditions for nonlifting configurations. This work focuses on comparisons with the free-flight data obtained in both the NASA Ames Research Center (ARC) Hypervelocity Free Flight Aerodynamic Facility (HFFAF) [13] and the Eglin ARF [14]. In addition to comparisons between the two facilities, two distinct methods of reducing the measured trajectories to aerodynamic coefficients are available for the Eglin data: CADRA and the Aeroballistic Research Facility Data Analysis System (ARFDAS), developed by Hathaway and Whyte [28]. The range test configuration is an early Orion CM configuration with identical radii of curvature at the maximum diameter and rear shoulder (cf. Fig. 3). Two center-of-gravity locations were tested for the nonlifting configuration, and here we examine the $x_{\text{c.g.}} = 0.26D$ configuration.

A summary of the static and dynamic coefficients at $M_\infty = 1.25$ and 2.5, compared with ballistic-range data reductions for the Orion CM, is presented in Fig. 6. Note that the Orion CM typically follows the Apollo coordinate convention, in which the static aeroshell-forward trim location is $\alpha = 180$ deg, but the results are rotated here to maintain consistency with the previous section. At Mach 1.25, there are three range data reductions: the same orientation and position from the Eglin ARF reduced using CADRA and ARFDAS

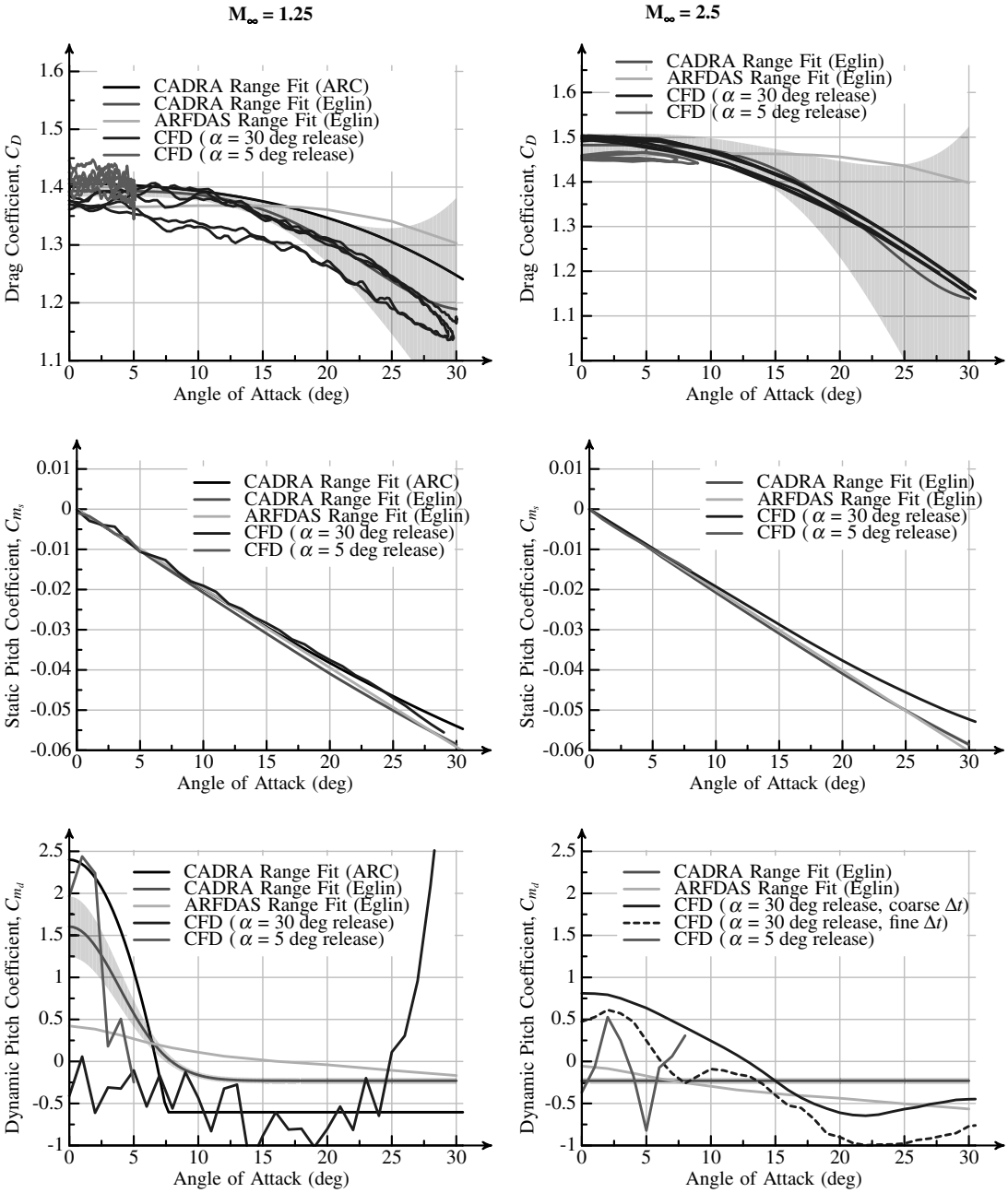

Fig. 6 Predictions of the static and dynamic (C_D, C_{m_s}, and C_{m_d}) aerodynamic coefficients for Orion CM configuration at two supersonic Mach numbers. Range data are the regression fit of an assumed aerodynamic model against the trajectory data [12], and 3σ uncertainties are included for the range data regression fit by assuming a uniform error distribution.

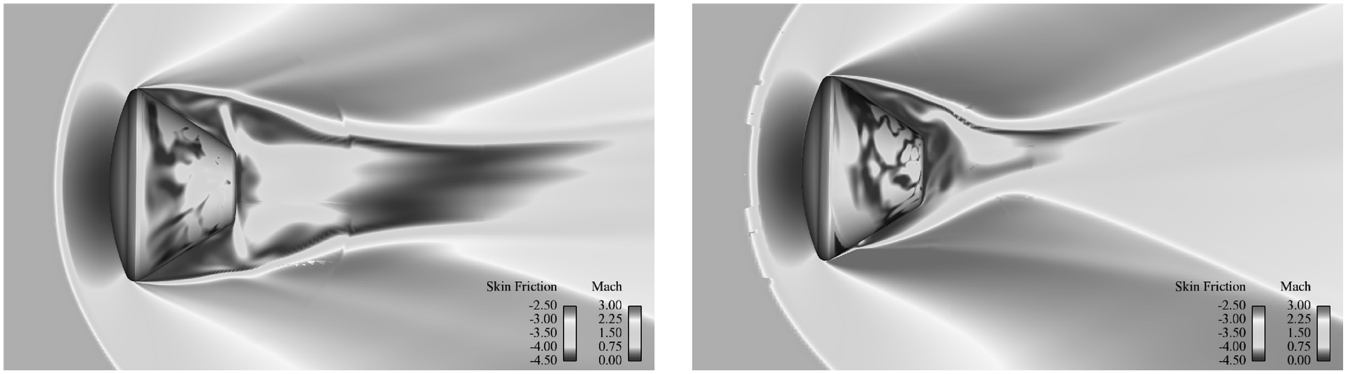

a) $\alpha = 0.8$ deg from $\alpha = 5$ deg release **b) $\alpha = 1.4$ deg from $\alpha = 30$ deg release**

Fig. 7 Snapshot of Mach contours along the lateral symmetry plane as the Orion CM passes through $\alpha = 0$ deg during free-oscillation simulations. The viscous surface is colored by $\log |C_f|$. Both simulations are pitching down (decreasing angle of attack). The Magnus effect in the higher α release (higher rotation rate) delays the separation around the maximum diameter location, leading to a shock-induced separation on the lower surface ($M_\infty = 2.5$, $Re_D = 3.5 \times 10^6$).

and a CADRA data reduction from the ARC HFFAF. Data were not taken in the ARC facility above $M_\infty = 1.25$. Multiple trajectories at conditions leading to both high-amplitude and low-amplitude oscillations are available in the range data. The data follow the same trends as the PAI-DAE analysis and only the main points are summarized again here. The drag coefficient is in good agreement with the range data reductions and shows a hysteresis at Mach 1.25. The slope of the static pitch coefficient is slightly lower in the higher-velocity simulations, compared with the range modeling. The damping demonstrates two distinct trends with release angle of attack (rotation rate), with the lower-angle-of-attack release showing a greater tendency toward instability (two angular resolutions are again included at $M_\infty = 2.5$). The stronger wake at Mach 1.25 leads to oscillatory damping predictions. The simulations predict a large damping coefficient at the high angles of attack for the $M_\infty = 1.25$ conditions. The rotation rate at these conditions is essentially zero, however, and so the value of the coefficient is arbitrary. Higher-amplitude data are necessary to get an accurate prediction for this regime. If a linear aerodynamic model is assumed for this regime, as is done in the range data reductions, the comparison is favorable. The different methods of reducing the range data and the data gathered from different ranges contain as much variation, especially for the dynamic damping coefficients near the static trim point and the drag coefficient at high angles of attack, as exists between the simulation data and the range predictions.

Figure 7 presents computed Mach contours and skin friction from two Mach 2.5 simulations differing by release angle of attack. In both simulations, the snapshot captures the body passing through the static trim point during the pitch-down (decreasing angle of attack) phase of the oscillation. The greater inertia of the boundary layer on the windward aeroshell (Magnus effect) due to the greater rotation rate in the higher α release delays the separation around the maximum diameter location, leading to a shock-induced separation on the smooth aftbody. The lower rotation rate separates near the location of maximum diameter, and the wake structure is much broader and stronger. This stronger wake leads to oscillations in the predicted damping coefficient, as is seen at the lower Mach numbers. The changing physical mechanisms with rotation rate are not reflected in common aerodynamic modeling approaches.

VI. Conclusions

The use of viscous free-oscillation computational fluid dynamics simulations to predict the aerodynamic behavior of capsule shapes in the supersonic-speed regime provides both the static and dynamic coefficients needed for aerodynamic modeling. The computed static coefficients are in good agreement with the available range data, and the computational and experimental dynamic coefficients follow the same trends. The predictive capability uses a static grid- and temporal-refinement strategy, along with the Spalart–Allmaras detached-eddy simulation turbulence model. The simulation results are validated for two novel configurations: an idealized inflatable decelerator concept and the Orion crew module. Analysis of the results indicates that the typical nonlinear bluff-body behavior is characterized by a rate-dependent dynamic response, which is not currently accounted for in common aerodynamic models. With this dynamic simulation approach, an aerodynamic performance database is generated using a fraction of the time required to build a typical static database while providing the dynamic response information needed for accurate modeling.

Acknowledgments

Jeff Brown of the ELORET Corporation and Leslie Yates of Aerospace Computing, Inc., assisted in gathering and cataloging the range data. Veronica Hawke of ELORET Corporation provided the CAD configurations for the Orion crew module. Finally, Michael Olsen of NASA Ames Research Center provided assistance in implementing and testing the k-ω lag model.

References

[1] Redd, B., Olsen, D. M., and Burton, R. L., "Relationship Between the Aerodynamic Damping Derivatives Measured as a Function of Instantaneous Angular Displacement and the Aerodynamic Damping Derivatives Measured as a Function of Oscillation Amplitude," NASA TN D-2855, June 1965.

[2] Moseley, W. C., Jr., Graham, R. E., and Hughes, J. E., "Aerodynamic Stability Characteristics of the Apollo Command Module," NASA TN D-4688, Aug. 1968.

[3] Steinberg, S., Uselton, B. L., and Siemers, P. M., III,, "Viking Pitch Damping Derivatives as Influenced by Support Interference and Test Techniques," *Journal of Spacecraft and Rockets*, Vol. 10, No. 7, July 1973, pp. 443–449. doi:10.2514/3.61906

[4] Sammonds, R. I., and Kruse, R. L., "Viking Entry Vehicle Aerodynamics at $M = 2$ in Air and Some Preliminary Test Data for Flight in CO_2 at $M = 11$," NASA TN D-7974, June 1975.

[5] Chapman, G. T., and Yates, L. A., "Dynamics of Planetary Probes: Design and Testing Issues," AIAA Paper 1998-0797, Jan. 1998.

[6] Chapman, G. T., and Yates, L. A., "Limit Cycle Analysis of Planetary Probes," AIAA Paper 1999-0496, Jan. 1999.

[7] Winchenbach, G. L., Chapman, G. T., Hathaway, W., Ramsey, A., and Berner, C., "Dynamic Stability of Blunt Atmospheric Entry Configurations," *Journal of Spacecraft and Rockets*, Vol. 39, No. 1, Jan. 2002, pp. 49–55. doi:10.2514/2.3781

[8] Murman, S. M., and Aftosmis, M. J., "Dynamic Analysis of Atmospheric-Entry Probes and Capsules," AIAA Paper 2007-0074, Jan. 2007.

[9] Buning, P. G., Chiu, I. T., Obayashi, S., Rizk, Y. M., and Steger, J. L., "Numerical Simulation of the Integrated Space Shuttle Vehicle in Ascent," AIAA Paper 88-4359, 1988.

[10] Jespersen, D. C., Pulliam, T. H., and Buning, P. G., "Recent Enhancements to OVERFLOW," AIAA Paper 97-0644, Jan. 1997.
[11] Nichols, R. H., Tramel, R. W., and Buning, P. G., "Solver and Turbulence Model Upgrades to OVERFLOW 2 for Unsteady and High-Speed Applications," AIAA Paper 2006-2824, 2006.
[12] Yates, L. A., and Chapman, G. T., "Analysis of Data from Ballistic Range Tests of PAI-DAE Vehicles," Aerospace Computing, Inc., Mountain View, CA, Nov. 2007.
[13] Brown, J. D., Bogdanoff, D. W., Yates, L. A., and Chapman, G. T., "Free-Flight Dynamic Aero Data for a Lifting CEV Capsule," AIAA Paper 2008-1232, Jan. 2008.
[14] Yates, L. A., and Chapman, G. T., "Analysis of Data from Ballistic Range Tests for an Untrimmed CEV Model," Aerospace Computing, Inc., Mountain View, CA, Dec. 2006.
[15] "Aerodynamic Results: NASA-CEV Test Configuration," Arrow Tech Associates, Rept. ARO-07-0111, South Burlington, VT, Jan. 2007.
[16] Kalviste, J., "Use of Rotary Balance and Forced Oscillation Test Data in Six Degrees of Freedom Simulation," AIAA Paper 1982-1364, 1982.
[17] Spalart, P. R., "Strategies for Turbulence Modeling and Simulations," *International Journal of Heat and Fluid Flow*, Vol. 21, No. 3, 2000, pp. 252–363. doi:10.1016/S0142-727X(00)00007-2
[18] Olsen, M. E., and Coakley, T. J., "The Lag Model, a Turbulence Model for Non Equilibrium Flows," AIAA Paper 2001-2564, June 2001.
[19] Chaderjian, N. M., and Olsen, M. E., "Grid Resolution and Turbulence Model Effects on Space Capsule Navier–Stokes Simulations," AIAA Paper 2007-4562, June 2007.
[20] Olsen, M. E., Chaderjian, N. M., Lillard, R. P., Greathouse, J. S., and Coakley, T. J., "Numerical Study of Massively Separated Flows," AIAA Paper 2007-1412, Jan. 2007.
[21] Chan, W. M., Gomez, R. J., Rogers, S. E., and Buning, P. G., "Best Practices in Overset Grid Generation," AIAA Paper 2002-3191, June 2002.
[22] Murman, S. M., "Dynamic Viscous Simulations of Atmospheric-Entry Capsules," AIAA Paper 2008-6911, August 2008.
[23] Hughes, S. J., Dillman, R. A., Starr, B. R., Stephan, R. A., Lindell, M. C., Player, C. J., and Cheatwood, F. M., "Inflatable Re-Entry Vehicle Experiment (IRVE) Design Overview," AIAA Paper 2005-1636, 2005.
[24] Yates, L. A., "A Comprehensive Aerodynamic Data Reduction System for Aeroballistic Ranges," Wright Lab., TR 96-7059, Dayton, OH, Oct. 1996.
[25] Spalart, P. R., Deck, S., Shur, M. L., Squires, K. D., Strelets, M. Kh., and Travin, A., "A New Version of Detached-Eddy Simulation, Resistant to Ambiguous Grid Densities," *Theoretical and Computational Fluid Dynamics*, Vol. 20, No. 3, 2006, pp. 181–195. doi:10.1007/s00162-006-0015-0
[26] Teramoto, S., Hiraki, K., and Fujii, K., "Numerical Analysis of Dynamic Stability of a Reentry Capsule at Transonic Speeds," *AIAA Journal*, Vol. 39, No. 4, 2001, pp. 646–653. doi:10.2514/2.1357
[27] Teramoto, S., and Fujii, K., "Mechanism of Dynamic Instability of a Reentry Capsule at Transonic Speeds," *AIAA Journal*, Vol. 40, No. 12, 2002, pp. 2467–2475. doi:10.2514/2.1590
[28] Hathaway, W. H., and Whyte, R. H., "Aeroballistic Research Facility Free Flight Data Analysis Using the Maximum Likelihood Method," Air Force Armament Laboratory, TR 79-98, Dec. 1979.

R. Cummings
Associate Editor